

Fission of U^{238} by 2.2-GeV Protons*

V. P. CRESPO,† J. B. CUMMING, AND A. M. POSKANZER‡

Chemistry Department, Brookhaven National Laboratory, Upton, New York 11973

(Received 18 March 1968)

Angular distributions and differential range curves at angles of 15° , 90° , and 165° have been obtained by radiochemical methods for several representative products which recoil out of thin uranium targets irradiated with 2.2-GeV protons. Mean momenta observed at 90° to the beam direction are 133, 125, and 125 (MeV amu) $^{1/2}$ for the neutron-excess isotopes Ba^{140} , Mo^{99} , and Sr^{91} , but only 96 and 104 (MeV amu) $^{1/2}$ for the neutron-deficient products Ba^{131} and Pd^{103} . The neutron-deficient isotopes have broader momentum distributions and more forward-peaked angular distributions than do the neutron-excess products. Results are discussed in terms of a two-step vector model, i.e., a fast nucleonic cascade followed by fission or another slower de-excitation step. The observed spectra and angular distributions for all the isotopes are consistent with such a model. Observed mean velocities are compared to those predicted by a liquid-drop theory of fission. It is concluded that products in the mass-90-to-140 range are produced primarily by a conventional fission mechanism. However, some contribution of a spallationlike process appears necessary to account for low-velocity fragments in the case of the neutron-deficient products (particularly Ba^{131}).

I. INTRODUCTION

THE interaction of high-energy protons with complex nuclei has commonly been discussed in terms of a two-step model in which the incident particle and its various collision partners interact with the nucleons in the nucleus in a quasifree manner.¹ This leads to the development of a fast nucleonic cascade with the ejection of nucleons or small groups of nucleons. The second step of the reaction is then the de-excitation of the various excited nuclei formed by the prompt cascade. For heavy-element targets such as uranium, fission will play an important role in competition with particle evaporation in this de-excitation step.

Examination of the mass-yield curve of uranium suggests a phenomenological division of products into three groups. Those nuclides with mass above 190 are *spallation residues* which result from de-excitation without fission of the excited nuclei produced by the fast nucleonic cascade. Nucleons and small aggregates of nuclear matter which are either ejected during the fast cascade or evaporated subsequently define a region of *emitted particles* which extends up to $A \approx 45$. Of particular interest in this region are products such as Na^{24} and Mg^{28} , whose excitation functions rise rapidly for bombarding energies above ≈ 0.5 GeV. The term *fragmentation* has been applied^{2,3} to the process leading to their formation. Some experimental data^{4,5} indicate

they are formed at times comparable to the development of the fast cascade. On the other hand, other data^{6,7} give evidence for a statistical mechanism (evaporation) playing an important role in their production.

The third region, $45 < A < 190$, contains *fission products*. A prominent fission peak is observed⁸ in this mass range at energies up to 28 GeV. The results of Debeauvois *et al.*⁹ at 18 GeV indicate that *binary fission* is the dominant process with *ternary fission* amounting to $\approx 2\%$ of the binary events. Comparison of their results, obtained with plastic foil detectors sensitive to masses greater than ≈ 20 , with those of Brandt *et al.*,¹⁰ who used Mica detectors sensitive to $A \gtrsim 30$, indicates that virtually all the ternary events observed by Debeauvois *et al.* had one fragment with mass in the ≈ 20 to ≈ 30 range. However, the frequency of ternary events is too low to account for a major part of the observed yield of fragmentation products. Ternary fission is extremely rare at a bombarding energy of 0.5 GeV.¹⁰ On the basis of studies of the recoil properties of products ranging from $Sc^{47,48}$ to Ba^{140} , Sugarman *et al.*¹¹ have concluded that the fission of uranium by 0.45-GeV protons can be described by a rather simple picture entailing a constant average distance, 18.4 F, between the charge centers of the primary fragments at scission. By comparison with results from studies of fission induced by a variety of other particles, i.e., heavy ions, α 's, they concluded that nuclear de-

* This research performed under the auspices of the U. S. Atomic Energy Commission.

† Present address: Estudos Gerais Universtarios de Mozambique, C. P. 257, Lourenço Marques, Portuguese East Africa.

‡ Present address: Lawrence Radiation Laboratory, University of California, Berkeley, Calif. 94720.

¹ For a general summary of high-energy reactions with an emphasis on fission, see E. K. Hyde, *The Nuclear Properties of the Heavy Elements* (Prentice Hall, Inc., Englewood Cliffs, N. J., 1964), Vol. III.

² R. Wolfgang, E. W. Baker, A. A. Caretto, J. B. Cumming, G. Friedlander, and J. Hudis, *Phys. Rev.* **103**, 394 (1956).

³ A. A. Caretto, J. Hudis, and G. Friedlander, *Phys. Rev.* **110**, 1130 (1958).

⁴ V. P. Crespo, J. M. Alexander, and E. K. Hyde, *Phys. Rev.* **131**, 1765 (1963).

⁵ J. B. Cumming, R. J. Cross, Jr., J. Hudis, and A. M. Poskanzer, *Phys. Rev.* **134**, B167 (1964).

⁶ I. Dostrovsky, Z. Fraenkel, and J. Hudis, *Phys. Rev.* **123**, 1452 (1961).

⁷ I. Dostrovsky, R. Davis, Jr., A. M. Poskanzer, and P. L. Reeder, *Phys. Rev.* **139**, B1513 (1965).

⁸ G. Friedlander, *Physics and Chemistry of Fission* (International Atomic Energy Agency, Vienna, 1965), Vol. II, p. 265.

⁹ M. Debeauvois, R. Stein, J. Ralarosy, and P. Cüer, *Nucl. Phys.* **A90**, 186 (1967).

¹⁰ R. Brandt, F. Carbonara, E. Cieslak, M. Dokowski, Ch. Gfeller, H. Piekarz, J. Piekarz, W. Riezler, R. Rinzivillo, E. Sassi, M. Sowinski, and J. Zakrzewski, *Nucl. Phys.* **A90**, 177 (1967).

¹¹ N. Sugarman, H. Münzel, J. A. Panontin, K. Wielgoz, M. V. Ramaniah, G. Lange, and E. Lopez-Mencher, *Phys. Rev.* **143**, 952 (1966).

formation at scission for high-energy fission processes is independent of excitation energy or mode of formation of the fissioning nucleus.

The above assignment of mechanisms on the basis of product mass is quite satisfactory at energies below ≈ 0.5 GeV. However, as bombarding energies increase into the GeV region the situation is much less clear cut. Friedlander⁸ has summarized a variety of cross-section measurements and obtained mass-yield curves for uranium at 2.9 and 28 GeV. A single broad fission peak centered at $A \approx 110$ is observed at both energies. However, its height is reduced and the valleys separating it from other mass regions are substantially filled in compared with lower energies. It is apparent that, at least in some mass regions, two or more mechanisms may contribute to product formation.

Measurements of charge-dispersion curves¹²⁻¹⁵ at energies above ≈ 0.6 GeV give double-peaked curves for masses in the 115 to 140 range, suggesting a contribution of at least two mechanisms. The neutron-excess peak is similar in position to the single peak observed in fission produced by ≈ 50 -MeV protons. For products in the $A=100-117$ region, experimental results¹⁶ at 2.9 and 28 GeV are consistent with either single- or double-peaked charge-dispersion curves. At $A=72$ ¹⁷ the curve has a single maximum at both 2.9 and 28 GeV.

Thick-target recoil studies^{12,13,18} of uranium fission induced by GeV protons give additional evidence for two mechanisms. These have shown that the neutron-deficient products have markedly smaller ranges than the excess ones. This is most dramatically seen in the results of Brandt,¹⁸ where the more neutron-deficient iodine and bromine isotopes at 18 GeV have $\approx \frac{1}{2}$ the mean ranges of the neutron-excess isotopes. For iodine the transition is abrupt at mass 123 and tends to confirm the distinctiveness of the two mechanisms. At 0.55 GeV, the neutron-deficient products have only slightly smaller mean ranges than the excess ones.

There is little doubt that the neutron-excess products in the middle mass region are formed by binary fission processes even at energies in the GeV region: they are produced in intranuclear cascades leading to low deposition energies. Neutron-deficient products, to the extent that they are produced at energies up to ≈ 0.7 GeV, appear to be produced by a similar process with larger deposition energies. On the basis of a comparative study of iodine isotope production from a variety of

targets at a bombarding energy of 18 GeV, Rudstam and Sorenson¹⁴ have concluded that the neutron-deficient iodine isotopes are produced from uranium by a "spallation-type" mechanism. They point out, however, that such a mechanism may also involve fragment emission and/or nonequilibrium evaporation. On the other hand, Alexander *et al.*¹³ conclude the same isotopes are produced by a fast process possibly correlated with fragmentation.

In the present work, thin-target recoil techniques of the type previously used to study Na²⁴ production from aluminum¹⁹ and bismuth⁵ have been applied to the investigation of the high-energy fission of uranium. Observed spectra and angular distributions are discussed in terms of the two-step vector model, extensively developed by Sugarman and co-workers^{20,21} and by Winsberg.²²

The two-step model describes the velocity \mathbf{v}_i of a particular recoil in the laboratory system as a sum of vectors,

$$\mathbf{v}_i = \mathbf{v} + \mathbf{V}. \quad (1)$$

The vector \mathbf{v} is a characteristic of the first step (cascade) of the reaction and \mathbf{V} is a characteristic of the second (fission or evaporation) step. In high-energy reactions, \mathbf{v} need not lie along the beam direction but may have a component v_{\perp} perpendicular to that direction, as well as a parallel component v_{\parallel} . It is convenient to define $\eta_{\parallel} = v_{\parallel}/V$ and $\eta_{\perp} = v_{\perp}/V$. It is a fundamental assumption of the vector model that the two steps of the reaction are sufficiently well separated so that memory of the beam direction, except for angular momentum effects, is lost at the time of the second step. If this is the case, the angular distribution of \mathbf{V} in the moving system should be, on the average, symmetric about 90° to the beam.

In Sec. II we discuss the experimental procedures and analyze the results to obtain the vector-model parameters of interest. Tests of the fundamental assumption of symmetry of the angular distribution about 90° are also made. Comparison of the quantities derived in Sec. II with those from other experiments is given in Sec. III together with discussions of possible mechanisms responsible for the product formation.

II. EXPERIMENTAL PROCEDURES AND RESULTS

A. General

Angular distributions and range spectra were measured for fission products recoiling out of thin uranium targets irradiated with 2.2-GeV protons in the Brook-

¹² G. Friedlander, L. Friedman, B. Gordon, and L. Yaffe, *Phys. Rev.* **129**, 1809 (1963).

¹³ J. M. Alexander, C. Baltzinger, and M. F. Gazdik, *Phys. Rev.* **129**, 1826 (1963).

¹⁴ G. Rudstam and G. Sørensen, *J. Inorg. Nucl. Chem.* **28**, 771 (1966).

¹⁵ E. Hagebø, *J. Inorg. Nucl. Chem.* **29**, 2515 (1967).

¹⁶ N. T. Porile, *Phys. Rev.* **148**, 1235 (1966).

¹⁷ S. Kaufman, *Phys. Rev.* **129**, 1866 (1963); and (private communication) as quoted in Ref. 8.

¹⁸ R. Brandt, *Physics and Chemistry of Fission* (International Atomic Energy Agency, Vienna, 1965), Vol. II, p. 329.

¹⁹ A. M. Poskanzer, J. B. Cumming, and R. Wolfgang, *Phys. Rev.* **129**, 374 (1963).

²⁰ N. Sugarman, M. Campos, and K. Wielgoz, *Phys. Rev.* **101**, 388 (1956).

²¹ N. T. Porile and N. Sugarman, *Phys. Rev.* **107**, 1410 (1957).

²² L. Winsberg, University of California Radiation Laboratory Report No. UCRL-8618, 1958, p. 44 (unpublished).

haven cosmotron. Selected for study were Ba^{131} ($N/Z=1.339$), a typical neutron-deficient product in the mass region where the double-humped charge-dispersion curve is well established, and Pd^{103} ($N/Z=1.239$), a neutron-deficient product of lower mass. For comparison, the neutron-excess nuclides Ba^{140} ($N/Z=1.500$) and Mo^{99} ($N/Z=1.357$) were also investigated. One spectrum was obtained for the neutron-excess product Sr^{91} as well. All of these isotopes represent cumulative yields of appropriate neutron-excess or -deficient chains since sufficient time elapsed between the end of irradiation and chemical separation to allow their precursors to decay. From the charge-dispersion data^{8,16} it can be estimated that the cumulative yields of Ba^{140} , Ba^{131} , Pd^{103} , and Mo^{99} will account for about 35, 35, 10, and 70% of the total isobaric yields of their respective mass chains.

The apparatus and irradiation techniques were basically the same as have been described previously.^{5,19} Targets were $\frac{1}{2}$ -in. squares of vacuum-deposited uranium supported by 0.0005-in. nickel foils (≈ 1.1 mg/cm²) or by ≈ 0.2 -mg/cm² Formvar. The standard uranium thickness was ≈ 0.17 mg/cm². As will be seen below, this thickness may be considered thin for the recoils of interest. Catcher foils were Mylar, 0.001 in. thick (≈ 3.5 mg/cm²) for the angular distribution measurements or 0.00015 in. thick (≈ 0.5 mg/cm²) for the range measurements.

Appropriate areas cut from the catchers after irradiation were dissolved in nitric and perchloric acid mixtures containing carriers for the elements of interest (Mo, Pd, and Ba). These elements were then separated and purified by combinations of steps taken from existing chemical procedures.²³ Difficulties were encountered in obtaining reproducible results for Mo unless both ion exchange (on Dowex-1) and solvent extraction (from 6*N* HCl with ethyl ether) steps were included. When the extraction was not included, the Mo samples showed substantial β contamination which decayed with a half-life of ≈ 7 h, although the longer-lived Mo^{99} appeared to be clean. The addition of $NaBrO_3$ during the Mylar dissolution and prior to the solvent extraction appeared to be necessary to promote exchange with the carrier and oxidize Mo to the hexavalent state. Final precipitation of the Mo with 8-hydroxy quinoline rather than as lead molybdate also appeared to improve reproducibility.

Inclusion of Ra in the Ba samples led to some difficulties. Ba^{131} and Ba^{140} were determined by milking their daughter activities Cs^{131} and La^{140} after a growth period

of ≈ 12 days. The Cs samples showed no interfering activities, but the La samples showed a variety of activities due to daughters of Ra isotopes. These were mostly removed by lead and bismuth sulfide scavengers leaving only 10-day Ac^{225} and its 3.3-h Pb^{209} daughter. A small background of activity from the carrier, probably Ac^{227} , was also observed with lanthanum from several different sources. In general, neither Ac^{225} nor Ac^{227} interfered appreciably with the La^{140} determinations other than to increase the errors somewhat.

Pd^{103} and Cs^{131} were assayed with x-ray spectrometers using thin NaI(Tl) crystals coupled to single-channel pulse-height analyzers. β particles from Mo^{99} were detected in end-window flow proportional counters. Aluminum absorbers (≈ 52 mg/cm²) were used to remove conversion electrons. The La^{140} was assayed in low-background β counters. In one experiment, Sr was separated instead of Pd. Sr^{91} in these samples was also assayed by β counting. The results of all the radioassays were corrected for decay, chemical yields, relative counter efficiencies, and sample thickness variations where appropriate. Because chemical yields were generally high and reproducible, the latter effects were generally small.

B. Angular Distributions

Angular distributions were measured with 15° resolution for Ba^{140} , Ba^{131} , Pd^{103} , and Mo^{99} . The activation blank as measured in a layer of catchers behind the first (ranges > 3.5 mg/cm²) was always less than 1% indicating no appreciable number of long-range recoils. Duplicate experiments in which the catcher foils subtended angles from 7.5° to 97.5° to the beam direction were arbitrarily normalized to give optimum overlap at the six angles from 15° to 90°. Another set of experiments was similarly performed with the catcher assembly rotated by 180° to cover the backward angles. The forward and backward halves of the angular distributions were joined at the 90° points which they had in common. The over-all normalization of the data is such that an integration over the angular distribution would yield the value 4π . From the agreement between duplicates at the various angles, standard deviations of a single determination are inferred to be 2.4, 2.5, and 3.4% for the Ba^{140} , Ba^{131} , and Pd^{103} data, respectively. These are consistent with the errors arising from chemical yield determinations, foil cutting, and counting statistics. Data for Mo^{99} showed much greater scatter than could be accounted for by these sources. This erratic behavior is believed to have several causes: contamination of the Mo by isotopes of some heavier element; exchange and/or chemical yield difficulties; and some problems with counting Mo^{99} in lead molybdate samples. These troubles were remedied gradually during the experiment but not until the angular distribution measurements were completed.

²³ For general compilations from which the various steps were taken, see the following reports of the National Academy of Sciences-National Research Council (available from Clearinghouse for Federal Scientific and Technical Information, U. S. Department of Commerce, Springfield, Va.): E. M. Scadden and N. E. Ballou, U. S. At. Energy Comm. NAS-NS 3009 (1960); D. N. Sunderman and C. N. Townley, *ibid.* 3010 (1960); P. C. Stevenson and W. E. Nervik, *ibid.* 3020 (1961); H. L. Finston and M. T. Kinsley, *ibid.* 3035 (1961); O. T. Høgdahl, *ibid.* 3052 (1961).

TABLE I. Quantities derived from the angular distributions, 2π experiments, and the spectra. Velocity units are (MeV/amu)^{1/2}.

	Ba ¹⁴⁰	Ba ¹³¹	Isotope Pd ¹⁰³	Mo ⁹⁹
F/B (ang. dist.)	1.083±0.024	1.340±0.024	1.278±0.052	(1.16 ±0.09)
F/B (2π expt)	1.036±0.035	1.324±0.027	1.227±0.094	1.086±0.018
F/B (mean)	1.068±0.020	1.329±0.023	1.270±0.048	1.086±0.018
$\langle\eta_{11}\rangle$	0.031±0.009	0.141±0.018	0.119±0.019	0.041±0.008
b/a^*	-0.150±0.018	-0.004±0.020	+0.003±0.022	...
$\langle v_{11}\rangle = \langle v_i \cos\theta_i \rangle$	0.028±0.008	0.080±0.008	0.101±0.010	...
$\langle v_{11}\rangle \approx \langle\eta_{11}\rangle/\langle V^{-1}\rangle$	0.029±0.008	0.084±0.005	0.106±0.017	0.050±0.010

* Calculated assuming $\langle\eta_{11}\rangle$ is zero. See text for a discussion of effects of nonzero $\langle\eta_{11}\rangle$.

Angular distributions for Ba¹⁴⁰, Ba¹³¹, and Pd¹⁰³ are plotted in Fig. 1. The angular distribution of the neutron-excess product, Ba¹⁴⁰, is strikingly different from those of the neutron-deficient products in that it shows preferred emission at sidewise angles even in the laboratory system. The distributions for Ba¹³¹ and Pd¹⁰³ peak in the forward direction, that of Ba¹³¹ slightly more so than that of Pd¹⁰³. Results for Mo⁹⁹ have not been included in Fig. 1. Despite their poor precision it was possible to conclude that the angular distribution of Mo⁹⁹ fell somewhere intermediate between those of Ba¹⁴⁰ and Pd¹⁰³. Integrated forward (F) to backward (B) intensity ratios were obtained from each angular distribution and are given in Table I. Errors on these F/B ratios are based on reasonable upper and lower limit curves which could be drawn in Fig. 1. and reflect the errors

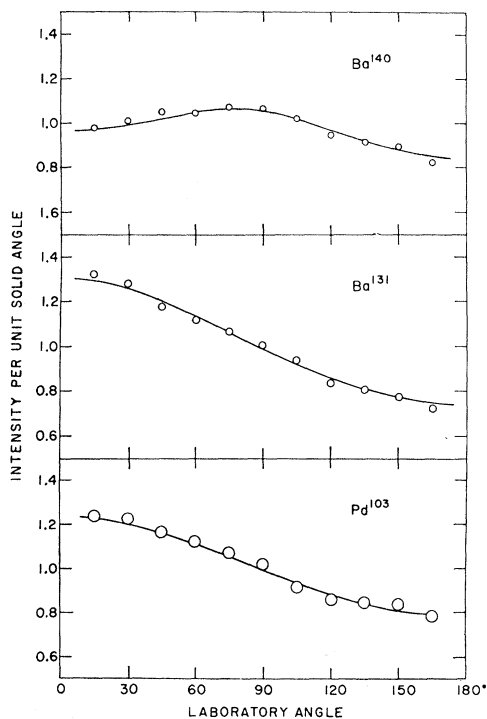


FIG. 1. Angular distributions in the laboratory system for Ba¹⁴⁰, Ba¹³¹, and Pd¹⁰³ from the 2.2-GeV proton-induced fission of uranium. Errors are estimated to be comparable to the size of the experimental points.

on the points inferred from the duplicate determinations. For reasons discussed above, the result for Mo⁹⁹ is highly uncertain.

To obtain a reliable F/B value for Mo⁹⁹, and as a check on the integrations of the Ba¹⁴⁰, Ba¹³¹, and Pd¹⁰³ angular distributions, four irradiations were performed with the catcher foils in a 2π geometry. Targets for these experiments were either ≈ 0.14 mg/cm² or ≈ 0.07 mg/cm² thick and were supported directly by either a forward or backward Mylar catcher (≈ 3.5 mg/cm²). Analysis of results obtained with the two target locations indicated that the fraction of recoils stopped in the targets was small and not significantly different from zero. (The largest observed value was 3.2% for Ba¹⁴⁰ in the 0.14-mg/cm² targets.) In calculating F/B , corrections were applied for the apparent retention in the targets and for blanks as well. No significant blanks were observed for Ba¹⁴⁰, Ba¹³¹, or Mo⁹⁹. However, blanks of 15 to 30% were observed for Pd¹⁰³. Such blanks would require unreasonable levels of impurities in the Mylar and their source could not be identified. Mean values of F/B from the 2π experiments are listed in Table I with errors based on reproducibility (except in the case of Pd¹⁰³ where a larger error is given to include uncertainties due to the large blanks). The F/B values are in reasonable agreement with those obtained from the angular distributions.

An angular distribution observed in the laboratory system depends primarily on the intrinsic angular distribution of \mathbf{V} in the moving system and on the quantity $\eta_{11} = v_{11}/V$ which determines the transformation between the two systems. To transform the observed angular distributions (Fig. 1) into the moving systems, we used trial values of $\langle\eta_{11}\rangle$ obtained from

$$\langle\eta_{11}\rangle = (F - B)/(F + B). \quad (2)$$

Transformed points are plotted in Fig. 2 at the appropriately transformed angles in the moving systems. Error flags on the points (1.7% for Ba¹⁴⁰, 1.8% for Ba¹³¹, and 2.4% for Pd¹⁰³) are based on reproducibility of the duplicate determinations at each angle. It is clear that the distributions for Ba¹³¹ and Pd¹⁰³ are isotropic within their errors, whereas that for Ba¹⁴⁰ shows a pronounced peak at 90°. Least-square fits of

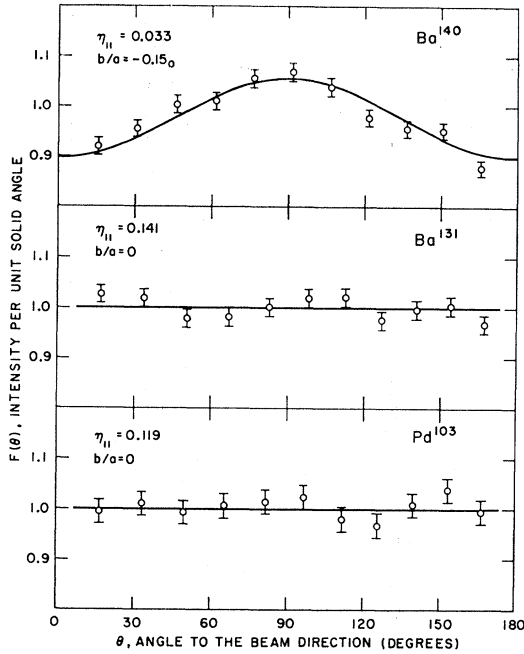


FIG. 2. Angular distributions for Ba^{140} , Ba^{131} , and Pd^{103} in the moving systems for which the forward-to-backward intensity ratios are unity. Values of $\langle\eta_{11}\rangle$ used for the transformation of the laboratory system data (Fig. 1) are indicated.

the transformed points to an angular distribution of the form

$$F(\theta) = a + b \cos^2\theta \quad (3)$$

gave values of $b/a = -0.150 \pm 0.018$ for Ba^{140} , -0.004 ± 0.019 for Ba^{131} , and $+0.003 \pm 0.018$ for Pd^{103} . For Ba^{140} we must now recalculate a value of $\langle\eta_{11}\rangle$, taking the anisotropy into account. Values of $\langle\eta_{11}\rangle$ and b/a and their errors as deduced from the angular distributions are given in Table I.

The angular distributions in Fig. 2 show no strong evidence for asymmetries of the sort expected¹⁹ if $\langle\eta_{\perp}\rangle$ were large. However, to investigate this quantitatively, each laboratory angular distribution was transformed for several sets of values of $\langle\eta_{11}\rangle$ and $\langle\eta_{\perp}\rangle$ and the transformed data fitted to Eq. (3) as before. The value of b/a for Ba^{140} was observed to be relatively insensitive to both $\langle\eta_{11}\rangle$ and $\langle\eta_{\perp}\rangle$. For $\langle\eta_{11}\rangle = 0.031$ and $\langle\eta_{\perp}\rangle = 0.124$, b/a increased slightly to -0.140 ± 0.018 . For both Ba^{131} and Pd^{103} , the anisotropies are essentially zero provided $\langle\eta_{\perp}\rangle \leq \langle\eta_{11}\rangle$. For larger values, small positive anisotropies would be inferred, e.g., for Ba^{131} with $\langle\eta_{11}\rangle = 0.141$ and $\langle\eta_{\perp}\rangle = 0.200$, $b/a = 0.025 \pm 0.018$. It is generally true that if one analyzes a particular distribution assuming different values of $\langle\eta_{\perp}\rangle$, the larger $\langle\eta_{\perp}\rangle$ will require larger values (more positive) of b/a for a best fit and vice versa. Due to this compensation it is not possible to choose a unique value for $\langle\eta_{\perp}\rangle$ on the basis of significantly improved fit of the transformed data points to Eq. (3).

C. Range Measurements

Differential range curves for Ba^{140} , Ba^{131} , Pd^{103} , and Mo^{99} were obtained at angles of 15° , 90° , and 165° to the beam direction. Catcher foils were 0.00015-in. Mylar ($\approx 0.5 \text{ mg/cm}^2$). The basic data obtained in these experiments are not tabulated in this paper but can be supplied by the authors on request. To investigate the effect of target thickness on the results, three irradiations were performed in the 165° orientation. Targets for these consisted of $\approx 0.38 \text{ mg/cm}^2$ U supported on 1.1 mg/cm^2 Ni, $\approx 0.17 \text{ mg/cm}^2$ U supported on 1.1 mg/cm^2 Ni, and 0.02 mg/cm^2 UF_4 supported on 0.05 mg/cm^2 Formvar. Probability plots (integral range curves) of the results of these irradiations are shown in Fig. 3. In all cases, one-half the thickness of the target in units of equivalent stopping power of Mylar has been added to the ranges. It is seen in Fig. 3 that results from the 0.02 mg/cm^2 target and the 0.17 mg/cm^2 target are virtually identical, but that there is evidence for broadening of the distributions obtained with the 0.38 mg/cm^2 target. The effect is more pronounced for the more sharply peaked distributions (Ba^{140} and Mo^{99}). For the duplicate range measurements at 15° and 90° and the angular distribution measurements, the standard $\approx 0.17 \text{ mg/cm}^2$ target thickness was used.

Examination of Fig. 3 indicates that the use of $\approx 0.5 \text{ mg/cm}^2$ catchers leads to relatively poor resolution, particularly in the case of Ba^{140} , where up to 97% of the recoils stop in one foil. Figure 3 shows that the range distribution of Ba^{131} is substantially broader than that of Ba^{140} and that a similar but less pronounced difference exists between Pd^{103} and Mo^{99} . Mean ranges for each species, calculated with the aid of a computer

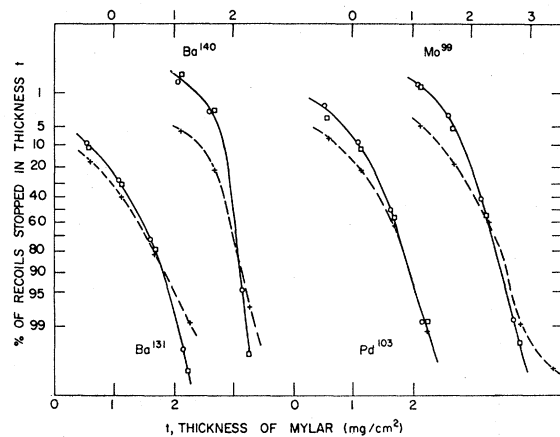


FIG. 3. Integral range curves obtained at an angle of 165° for Ba^{131} , Ba^{140} , Pd^{103} , and Mo^{99} recoiling out of various thickness uranium targets. The targets were as follows: +, 0.38 mg/cm^2 U supported by 1.1 mg/cm^2 Ni; \square , 0.17 mg/cm^2 U on 1.1 mg/cm^2 Ni; \circ , 0.02 mg/cm^2 UF_4 on 0.05 mg/cm^2 Formvar. The upper abscissa scales apply to Ba^{140} and Mo^{99} , the lower ones to Ba^{131} and Pd^{103} .

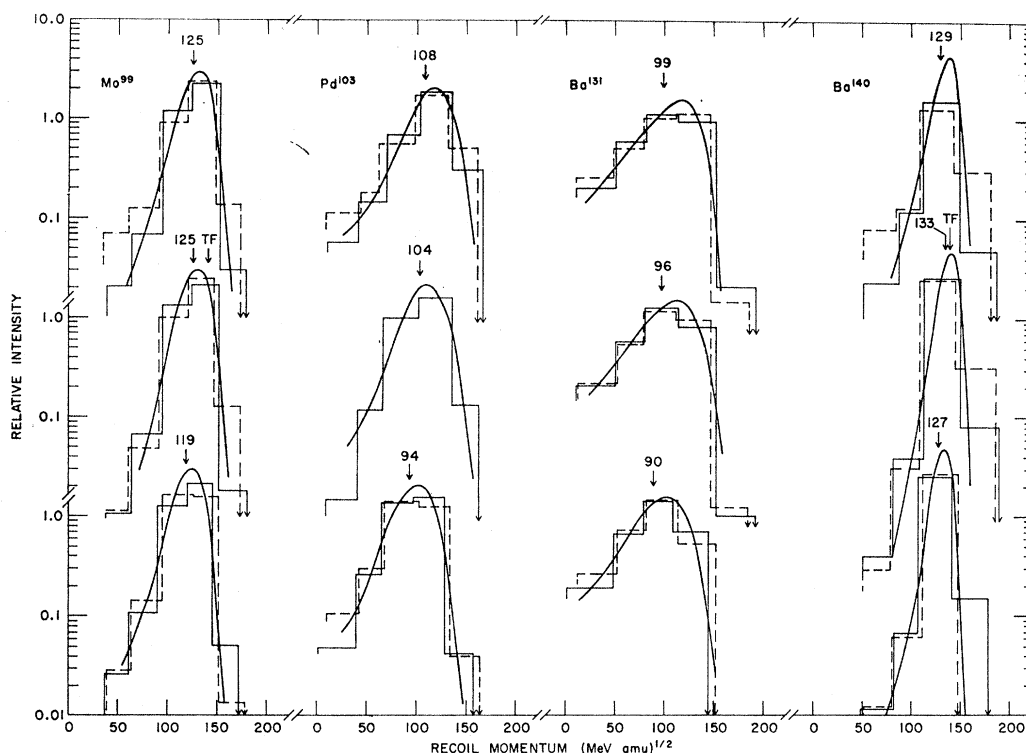


FIG. 4. Momentum spectra of Mo^{99} , Pd^{103} , Ba^{131} , and Ba^{140} from the 2.2-GeV proton-induced fission of uranium. The upper, center, and lower spectra for each isotope were obtained at angles of 15° , 90° and 165° to the beam, respectively. All spectra have been normalized to the same area but are displaced for different angles by factors of 100 for display purposes. The solid and dashed histograms are from duplicate irradiations. The curves are attempts to correct for the experimental resolution. Mean momenta are indicated by arrows surmounted by numbers. The arrows surmounted by TF are the values observed for Mo^{99} and Ba^{140} in the thermal fission of U^{235} .

program²⁴ which approximately corrected for the poor resolution, are listed in Table II. They show good reproducibility of duplicate experiments and demonstrate that a neutron-deficient species (Ba^{131} or Pd^{103}) in a given mass range has a significantly shorter mean range than a neutron-excess species (Ba^{140} , Mo^{99} , or Sr^{91}). This confirms the earlier thick-target results.^{12,13,18} It is interesting to note that the mean ranges for Ba^{140} and Mo^{99} are only slightly lower than those observed in Mylar²⁵ for these products from the thermal neutron-induced fission of U^{235} (range of $\text{Ba}^{140} = 2.11 \pm 0.04$ mg/cm², range of $\text{Mo}^{99} = 2.57 \pm 0.05$ mg/cm²).

For further analysis, the basic range data have been converted to momentum spectra using range-energy curves based on a semiempirical treatment of fission fragment stopping described elsewhere.²⁵ Momentum spectra for Ba^{140} , Ba^{131} , Pd^{103} , and Mo^{99} are presented in Fig. 4. Dashed and solid histograms refer to the first and second irradiations at each angle. (Data from the one irradiation at 165° with a thick target are not in-

cluded. Likewise the one spectrum obtained for Sr^{91} at 90° is not shown.) Agreement between duplicates is reasonably good. The most obvious disagreement appears between the two 15° irradiations where the dashed histograms appear broader than the solid ones. In calculating mean momenta and energies, we have weighted results from the broader distributions only one half as heavily as those from the narrower ones. The source of this broadening is not known but the result may reflect some damage to the target during the irradiation. The curves shown in Fig. 4 are based on integral momentum distributions. Smooth curves could be drawn through plots on probability paper of the integral data for Ba^{131} , Pd^{103} , and Mo^{99} with little ambiguity. Because of its relatively narrower range distribution, this was not the case for Ba^{140} .

Mean momenta and energies were obtained for each spectrum again using the computer program²⁴ to correct for the poor resolution. Results of the duplicate determinations were averaged and are presented in Table III together with estimates of the full widths of the momentum distributions [full width at half-maximum (FWHM)] obtained from the smooth curves of Fig. 4. Errors on the mean momenta due to errors from counting statistics, chemical yields, etc., are small ($\approx 0.5\%$). Errors due to foil thickness uncertainties cannot exceed

²⁴ In this program a Gaussian-like function is fit to a limited region of the curve (three points) and is then used to evaluate the derivatives of the curve. Resolution corrections are then calculated from the derivatives. If all recoils stopped in only three foils this would be equivalent to assuming a Gaussian shape for the entire curve. It is less restrictive when the recoils are spread over more foils.

²⁵ J. B. Cumming and V. P. Crespo, Phys. Rev. **161**, 287 (1967).

the $\approx 1\%$ deduced from the agreement of the duplicate results, particularly since, in the duplicates, the foils differed in thickness by a few percent. A more significant source of uncertainty in the momenta arises from the poor resolution of the experiment. The raw means (i.e., those calculated by assuming all events were concentrated at the center of each histogram) were within 2% of the corrected means. Furthermore, forcing Gaussian curves through three points of the Ba^{140} data gave means within 1% of the corrected means. Another source of error may arise from damage to the target resulting in a broadening of the momentum spectrum and a shift to lower values, e.g., note the $\approx 2\%$ lower ranges of the first irradiation at 15° compared to those from the second. We assign errors of 1.5% to the mean momenta of Ba^{131} , Pd^{103} , Mo^{99} , and Sr^{91} in Table III and 2% to those for Ba^{140} . Relative errors of the mean energies given in Table III are estimated to be approximately twice those of the mean momenta. These error estimates do not include contributions from uncertainties in the range-energy relationship. Preliminary analysis of the present data using a less-refined range-energy relation gave mean momenta which differed by -2 to $+6\%$ from those in Table III. We feel that the absolute accuracy of the range-energy treatment²⁵ used in this work should be better than 5% and that the relative accuracy in comparing momenta of different isotopes should be of the order of 2%.

Mean momenta are indicated by arrows in Fig. 4. For each isotope, the mean momentum at 15° is greater than at 165° as a consequence of v_{11} . Mean momenta at 90° are larger than the average of the momenta at 15° and 165° in all cases. For Ba^{140} the 90° mean is actually greater than the 15° mean. While the errors in the measurements are sufficiently large so no strong case can be based on this observation, it is in the direction expected from v_1 or a correlation between a variable anisotropy parameter and V .

The widths (FWHM) of the momentum distributions, although poorly determined in this experiment, indicate no strong dependence of spectral shape on angle of observation. Based on the 90° spectra, the neutron-deficient isotopes have significantly lower mean momenta and broader momentum distributions than the neutron-excess isotopes. The widths of the distributions for the more typical fission products Ba^{140} , Mo^{99} , and Sr^{91} are somewhat broader at 2.2 GeV than the 10 to 12% observed²⁵ for these isotopes in the thermal fission of U^{235} . Of particular interest in later discussions is the significant number of low-momentum recoils present in the Ba^{131} spectra and, to a lesser extent, in those of Pd^{103} .

By combining data from the spectra and angular distributions the mean value of v_{11} can be obtained. Provided the angular distribution of V is symmetric about 90° in the moving system, it can be shown that

$$\langle v_{11} \rangle = \langle v_1 \cos \theta_l \rangle = \langle v_{11} + V \cos \theta \rangle, \quad (4)$$

TABLE II. Mean ranges in Mylar for various products from the 2.2-GeV proton-induced fission of uranium.

Angle	Target thickness (mg/cm ²)	Corrected ^a mean range (mg/cm ²) for:				
		Ba ¹⁴⁰	Ba ¹³¹	Pd ¹⁰³	Mo ⁹⁹	Sr ⁹¹
15°	0.14	1.92	1.39	1.77	2.25	...
	0.18	1.94	1.44	1.82	2.28	...
90°	0.16	2.00	1.38	...	2.28	2.48
	0.14	1.99	1.38	1.72	2.27	...
165°	0.45	1.81	1.20	1.44	2.06	...
	0.20	1.90	1.29	1.56	2.16	...
	0.02	1.90	1.27	1.54	2.15	...

^a Values have been corrected for the thickness of the targets and the catcher foils as discussed in the text.

where the averaging includes all recoils hence is over both velocity and angle. Using the dependence of lab velocity v_l on angle θ_l as determined by the spectra and the observed angular distribution, the average of $v_l \cos \theta_l$ was obtained by numerical integration. Results for Ba^{140} , Ba^{131} , and Pd^{103} are given in Table I. Errors on the $\langle v_{11} \rangle$ values are estimates based on errors on the quantities entering into their calculation. An alternative way of obtaining $\langle v_{11} \rangle$ is to divide values of $\langle \eta_{11} \rangle$ obtained from the angular distributions by estimates of $\langle V^{-1} \rangle$ obtained from the spectra. This is inexact in that obtaining $\langle \eta_{11} \rangle$ from the angular distributions Eq. (2) was used and this is exact only if there are no $\eta_{11} > 1$. The assumption that $\eta_{11}/\langle V^{-1} \rangle = \langle v_{11} \rangle$ is also true only if there is no correlation between v_{11} and V . Values of $\eta_{11}/\langle V^{-1} \rangle$ listed in Table I are seen to be in good agreement with the values of $\langle v_l \cos \theta_l \rangle$.

D. Test of the Two-Step Model

To this point we have assumed the validity of the two-step vector model and its assumption of an angular distribution symmetric about 90° . By comparison of the spectra and angular distribution for a particular isotope, a test of this assumption should be possible. In a previous study⁵ it was concluded that the angular distribution of Na^{24} produced from bismuth by 2.9-GeV protons was inconsistent with the observed spectra and hence indicated a breakdown of the two-step model. One possible conclusion was that Na^{24} , a typical fragmentation product, was emitted in part before the ex-

TABLE III. Means of the momentum and energy distributions.

Angle	Ba ¹⁴⁰	Ba ¹³¹	Isotope Pd ¹⁰³	Mo ⁹⁹	Sr ⁹¹
Mean momentum ^a (MeV amu) ^{1/2}					
15°	128.9(19)	98.9(55)	108.3(40)	124.7(30)	...
90°	133.2(17)	96.2(60)	103.7(42)	125.2(31)	125.5(26)
165°	126.9(19)	89.6(56)	93.8(45)	118.8(31)	...
Mean energy (MeV)					
15°	62.1	41.5	60.7	80.9	...
90°	66.4	39.2	55.5	81.4	88.2
165°	60.8	33.9	45.8	73.4	...

^a Full widths of the momentum distributions are given in parentheses.

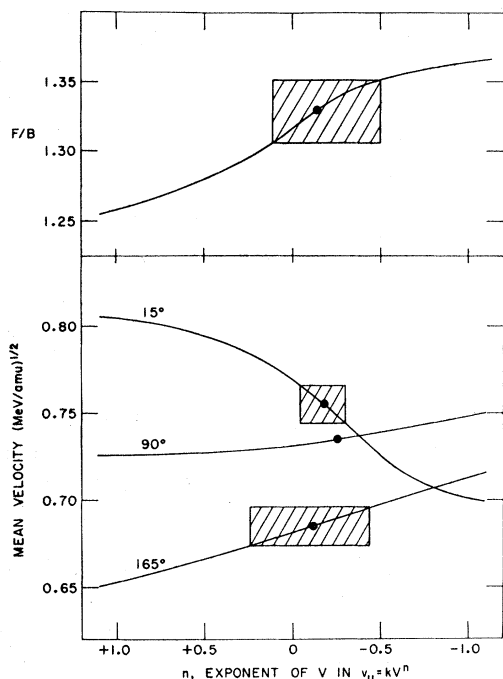


FIG. 5. Dependence of calculated mean velocities and the F/B ratio for Ba^{131} on the value of exponent n in the assumed correlation function $v_{11} = kV^n$. The shaded boxes denote regions consistent with the experimental values.

cited nucleus lost its memory of the beam direction. Since the neutron-deficient fission products have been postulated to be connected in some way with the fragmentation process, a similar test of the validity of a two-step model in their case is desirable.

A variety of exact or approximate relations have been developed which relate the various vector-model parameters to observable quantities in either thick- or thin-target recoil experiments. These have generally involved mean values rather than distributions; and for distributions such as available from these experiments, the closed form solutions are not readily obtained. We have used instead a reverse calculation in which assumed values of V , v_{11} , v_{\perp} , and b/a are used to calculate the observable quantities. The input parameters are then varied to achieve a match with the experimental values. Mean values of the various parameters as determined by direct calculation in the preceding sections furnish constraints to the region of parameter space to be investigated. We have programmed this as a Monte Carlo calculation for a high-speed digital computer. An outline of the calculation for one event is given below.

A value of V was selected from an integral probability distribution (supplied in tabular form) by choice of a random number. The cosine of the angle of V to the beam direction (z axis) was chosen to be randomly distributed by between $+1$ and -1 . However, if the anisotropy parameter was not zero, the distribution was appropriately weighted to conform to Eq. (3). Values

of v_{11} and v_{\perp} were selected and the angle of v_{\perp} to the plane defined by V and the beam was obtained from another random-number choice. The three vectors V , v_{11} , and v_{\perp} were added to give the laboratory velocity v_l , which was then binned on the basis of its magnitude and direction θ_l to the beam direction. For initial trials, 50 000 such calculations were performed to give velocity distributions at 15° , 90° , and 165° to the beam direction, the angular distribution of recoils, and the various average values of interest. When a good match with the observed quantities was obtained a few calculations with 10^6 events were performed to reduce the statistical errors.

Some of the points investigated in these calculations will be illustrated for Ba^{131} . A starting distribution for V was obtained from an approximate mean of the laboratory spectra. Since the effects of v_{\perp} are rather small, a unique value rather than a distribution was used. The effect of a distribution of v_{11} (uncorrelated with V) was examined and shown to give virtually identical results as using a unique value equal to $\langle v_{11} \rangle$. More significant effects are expected from correlations between v_{11} and V . We have assumed a correlation of the form

$$v_{11} = kV^n, \quad (4)$$

and calculated values of F/B and the mean velocities at 15° , 90° , and 165° as a function of the exponent n . For these calculations, k was adjusted to maintain $\langle v_{11} \rangle$ equal to 0.080 (the experimental value), $v_{\perp} = 0.100$, and $\langle V \rangle = 0.724$ $(\text{MeV}/\text{amu})^{1/2}$. Results are shown in Fig. 5. The effects noted may be explained most clearly in terms of the dependence of η_{11} on V . For $n=1$, $\eta_{11} = v_{11}/V$ is a constant and recoils with any particular V will have the same angular distribution in the laboratory system as any other value of V . For $n=0$ or -1 , $\eta_{11} = k/V$ or $\eta_{11} = k/V^2$ and those events corresponding to small values of V will be preferentially collimated in the forward direction in the laboratory. As a consequence, the mean velocity observed at 165° (and to a lesser extent that at 90°) and F/B rise with decreasing values of n and the mean velocity observed at 15° falls. It is interesting to note that only for $n \geq 1$ do the mean velocities at 15° and 165° approach $\langle V \rangle + \langle v_{11} \rangle$ and $\langle V \rangle - \langle v_{11} \rangle$, respectively. It was an underestimation of these correlation effects that led to a preliminary conclusion²⁶ that the production of Ba^{131} and Pd^{103} could not be accounted for by a two-step mechanism. The points shown in Fig. 5 are the intersections of the experimental values for Ba^{131} with the curves. Shaded boxes indicate ranges allowed by the experimental errors. The four measured quantities are seen to be consistent with a rather weak negative correlation ($n \approx -0.2$), hence we can account for the observed mean velocities and F/B on the basis of a two-step model. Further tests of this model can be made on the basis

²⁶ J. B. Cumming (unpublished).

of shapes of the velocity spectra and the angular distribution. To obtain the requisite statistical accuracy 10^6 events were calculated using a value of $n = -0.25$. The resulting velocity spectra are compared with the experimental data in Fig. 6. The agreement is very good. The shoulder seen on the low-velocity side of the 15° spectrum is a consequence of the collimation effect discussed above. The calculated angular distribution is the smooth curve drawn through the points in Fig. 1. Agreement is again good. Experimental values of F/B , $\langle v_l \rangle_{15^\circ}$, $\langle v_l \rangle_{90^\circ}$, and $\langle v_l \rangle_{165^\circ}$ are compared with those calculated in Table IV. To examine the dependence of these results on the form of the assumed correlation, a somewhat different form, $v_{11} = c + dV$, was investigated. Comparable fits to those based on Eq. (4) were obtained for small negative values of d .

The same general calculational procedure was applied to the Pd^{103} data. Curves analogous to those in Fig. 5 were obtained which again indicated a slight negative correlation between v_{11} and V . Since the spectrum of V for Pd^{103} is narrower than for Ba^{131} , the effects of the correlations are less pronounced and the case of v_{11} uncorrelated with V could not be ruled out. A value of $n = -0.25$ would be consistent with data for both isotopes. Some comparisons between experimental and calculated quantities for Pd^{103} are presented in Table IV. It is interesting that Winsberg²⁷ in an analysis of spallation reactions (Tb^{149} production from Ta, Bi, and Au) has also concluded that n is in the range 0 to -0.5 .

Since data are also available for the neutron-excess isotopes, it is of interest to see whether they too can be fitted by this model. Due to the narrower distributions of V for Ba^{140} and Mo^{99} compared to those of Ba^{131} and Pd^{103} , stronger correlations are necessary to achieve reasonable agreement between the experimental and calculated mean values. Rather larger values of $v_{11} = 0.172$ appear to be required to account for the abnormally large value of $\langle v_l \rangle$ observed at 90° for Ba^{140} . While the shape of the angular distribution calculated for Ba^{140} with $b/a = -0.15$ (the smooth curve in Fig. 1) is in reasonable agreement with the experimental data, the shapes of the velocity spectra leave something to be desired. However, it is felt that at least part of this difficulty arises from ignoring details of the distributions of v_{11} and v_l in calculations for cases such as Ba^{140} in which the distribution of V is quite narrow. The experimental results can probably be fitted within their errors if suitable distributions of v_{11} , v_l , V and b/a together with correlations between them are used in the calculation. We thus conclude that all the data are consistent with the two-step model.

III. DISCUSSION

In this section we will examine the results of the present experiment in more detail and compare them

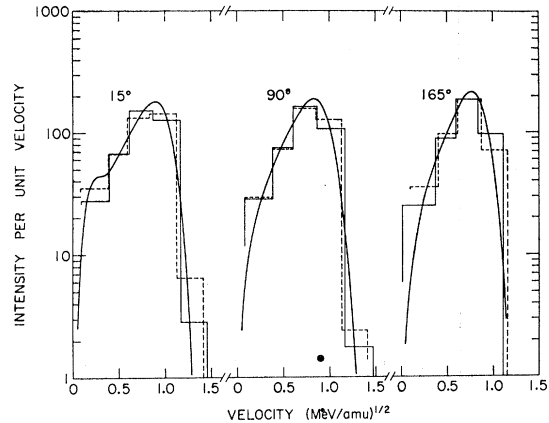


FIG. 6. Comparison of experimental with calculated velocity spectra for Ba^{131} . The histograms represent the experimental data. The smooth curves were calculated assuming a two-step model.

with those of other experimenters to see what information can be obtained concerning the reaction mechanisms leading to products in the middle mass region. As we have seen, angular distributions and spectra for the neutron-deficient products are consistent with a two-step mechanism and a small negative or zero correlation between v_{11} and V . While this cannot rule out a fast mechanism, it does suggest that the vector-model parameters may be appropriate to use even for these products.

A. Excitation Energies

The first step of a high-energy nuclear reaction leads to the production of a variety of excited nuclei having deposition energies E^* and forward components of momentum p_{11} . In a preceding section we have derived $\langle v_{11} \rangle$ for some specific products, hence $\langle p_{11} \rangle$ may be obtained if an assumption about the mass A of the excited nucleus is made. However, it is the value of E^* (as well as the A and Z of the excited nucleus) which determines the de-excitation or second step of the reaction. For example, the fission of uranium changes from predominantly asymmetric mass splits at low energies to predominantly symmetric fission at higher energies.²⁸ While kinematics can be used to obtain relations be-

TABLE IV. Comparison of experimental mean velocities at three angles and F/B with those calculated assuming a two-step model with a correlation of the form $v_{11} = kV^{-2.05}$. Velocity units are $(MeV/amu)^{1/2}$.

	Isotope			
	Ba^{131}		Pd^{103}	
	expt.	calc.	expt.	calc.
F/B	1.329 ± 0.023	1.325	1.270 ± 0.048	1.260
$\langle v_l \rangle_{15^\circ}$	0.755 ± 0.011	0.751	1.051 ± 0.016	1.054
$\langle v_l \rangle_{90^\circ}$	0.735 ± 0.011	0.737	1.007 ± 0.015	1.010
$\langle v_l \rangle_{165^\circ}$	0.685 ± 0.010	0.686	0.911 ± 0.014	0.916

²⁷ L. Winsberg, Phys. Rev. **135**, B1105 (1964).

²⁸ P. C. Stevenson, H. G. Hicks, W. E. Nervik, and D. R. Nethaway, Phys. Rev. **111**, 886 (1958).

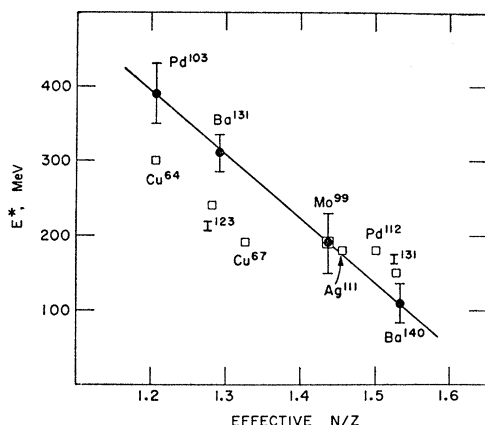


FIG. 7. Dependence of cascade deposition energy E^* on N/Z of products formed in the GeV proton irradiation of uranium. Filled circles are data obtained in this experiment. The squares represent results of Alexander *et al.* (see Ref. 13).

tween E^* and p_{11} if simple reaction mechanisms are assumed,^{29–31} relationships based on Monte Carlo calculations of the nucleonic cascade are of more general use. In particular, Porile's³² analysis of the calculations of Metropolis *et al.*³³ has been applied to the interpretation of a variety of recoil experiments. Recent Monte Carlo calculations by Chen *et al.*³⁴ have examined the dependence of the E^* - p_{11} relationship on the nuclear model used. They concluded that the E^* - p_{11} relation is not strongly dependent on the target nucleus, nuclear model, or bombarding energy, provided E^* is expressed in units of E_{\max} , the maximum excitation energy which would result if a compound nucleus were formed and p_{11} is in units of p_{inc} , the momentum of the incident proton. The distributions of E^* for a given p_{11} or of p_{11} for a given E^* are quite broad and as a consequence, different curves are obtained if $\langle E^* \rangle$ is plotted versus p_{11} or if $\langle p_{11} \rangle$ is plotted versus E^* . Virtually all recoil data have been interpreted in terms of a relation between $\langle p_{11} \rangle$ and E^* which is reasonably linear for values of $\langle p_{11} \rangle$ up to $\approx 0.5p_{\text{inc}}$. For conversion of $\langle p_{11} \rangle$ values from the present experiment, we have used the simple relationship $E^*/E_{\max} = 0.75\langle p_{11} \rangle/p_{\text{inc}}$. This is the same as was used by Alexander *et al.*¹³ in the analysis of their recoil data. We have assumed a mass of 230 in the conversion of $\langle v_{11} \rangle$ to $\langle p_{11} \rangle$. The resulting excitation energies are 110 ± 25 , 190 ± 40 , 310 ± 25 , and 390 ± 40 MeV for Ba^{140} , Mo^{99} , Ba^{131} , and Pd^{103} , respectively. The errors reflect the errors in $\langle v_{11} \rangle$ only and do not include uncertainties due to the E^* - $\langle p_{11} \rangle$ relation. For example, had we used the relationship between E^* and $\langle p_{11} \rangle$ de-

duced from the recent Monte Carlo calculations at 0.38 MeV³⁴ using the STEPNO³⁵ model, values of 120, 210, 340, and 420 MeV would be obtained. If the STEP³⁵ model is used, the corresponding values are 20, 120, 270, and 370 MeV. Still different values result if the relationship between $\langle E^* \rangle$ and p_{11} is used. It is apparent that, while E^* values are of use in qualitative discussions, detailed quantitative conclusions based on their values may be precarious.

Values of E^* are plotted as a function of neutron-to-proton ratio, N/Z , in Fig. 7. Since the observed products represent cumulative yields, N/Z values of the average precursor fragments as obtained from the charge-dispersion data of Friedlander *et al.*,¹² Porile,¹⁶ or Kaufman¹⁷ were used in the appropriate mass regions. Our results indicate that E^* increases with decreasing N/Z and that the slope of the E^* versus N/Z line is the same for $A \approx 135$ and $A \approx 100$ mass regions. While no strong conclusions can be drawn because we have only two points in each mass region, the existence of a universal curve is perhaps not unexpected. It has been observed¹² that when the energies at which excitation functions peak are plotted as a function of N/Z , results for $A \approx 130$ and $A \approx 85$ also fall on a single curve. The slope of the line in Fig. 7 is ≈ 860 MeV per unit change of N/Z .

Values of E^* obtained by Alexander *et al.*¹³ for several products from the 6.2-GeV irradiation of uranium are also included in Fig. 7. Agreement is good for the neutron-excess species. However, the results of Alexander *et al.*, for the neutron-deficient species are lower than those observed here. It is expected that thick-target measurements would lead to lower values of $\langle \eta_{11} \rangle$ than thin-target measurements when range distributions are broad as is the case of Ba^{131} and Pd^{103} . The results of Sugarman *et al.*¹¹ at 0.45 GeV are substantially lower than those of the present experiment, e.g., 53 MeV for Ba^{140} and 106 MeV for Mo^{99} . Results of Alexander *et al.* show very little dependence of E^* on bombarding energy in the range 0.72 to 6.2 GeV.

Figure 7 confirms that, as had been previously noted, the neutron-deficient products are formed in higher deposition energy processes than are the neutron-excess ones. At 2.2 GeV there does not, however, appear to be a clear-cut separation into two groups on the basis of E^* .

B. Anisotropies

From a classical point of view, anisotropies of fission fragment angular distributions reflect preferred emission of fragments in a plane perpendicular to the direction of the angular momentum vector. For fission following compound-nucleus formation, the angular momentum vectors will be preferentially oriented perpendicular to the beam direction and the fragment anisotropies are

²⁹ S. C. Fung and I. Perlman, *Phys. Rev.* **87**, 622 (1952).

³⁰ A. Turkevich, quoted in Ref. 21.

³¹ T. Ericson, F. Selleri, and R. T. van de Walle, *Nucl. Phys.* **36**, 353 (1962).

³² N. T. Porile, *Phys. Rev.* **120**, 572 (1960).

³³ N. Metropolis, R. Bevins, M. Storm, A. Turkevich, J. M. Miller, and G. Friedlander, *Phys. Rev.* **110**, 185 (1958).

³⁴ K. Chen, Z. Fraenkel, G. Friedlander, J. R. Grover, J. M. Miller, and Y. Shimamoto, *Phys. Rev.* **166**, 949 (1968).

³⁵ The terms STEP and STEPNO describe the nuclear model used in the calculation. The nuclear density distribution is approximated by series of steps in both. Particle refraction and reflection are included in STEP but not in STEPNO.

expected to be positive, i.e., emission at 0° and 180° is favored. The anisotropy is expected to decrease with increasing excitation of the fissioning nucleus but to increase with increasing angular momentum. Theoretical treatments by Bohr³⁶ and Halpern and Strutinski³⁷ are in general agreement with experimental results at low energies.

The situation in high-energy nuclear reactions is considerably more complicated, because cascades result in the production of a variety of excited nuclei whose angular momentum vectors vary widely in both magnitude and direction. Over-all fission fragment anisotropies at bombarding energies of ≈ 0.6 GeV are near zero.^{38,39} However, Sugarman *et al.*¹¹ have observed significant anisotropies for a number of specific fission products at 0.45 GeV. The anisotropy parameter observed for Ba¹⁴⁰ in the present work, -0.15 ± 0.02 , is identical within errors with the value at 0.45 GeV, -0.108 ± 0.028 , and indicates at least some anisotropies persist to an energy of 2.2 GeV.

Sugarman *et al.*¹¹ have concluded from their data that there is a general correlation of the anisotropy parameter with deposition energy, with b/a negative for low values of E^* (≈ -0.1 for deposition energies ≈ 50 MeV) and positive for large deposition energies ($\approx +0.1$ for $E^* \approx 200$ MeV). Since virtually no anisotropy was observed for Ba¹³¹ and Pd¹⁰³ in the present experiment despite E^* values in excess of 300 MeV, it appears the same correlation between b/a and E^* observed at 0.45 GeV does not hold at 2.2 GeV.

Sufficient information is contained in the output from the recent Monte Carlo calculations³⁴ of the nucleonic cascade to allow calculation of angular distributions of the angular momentum vectors resulting from the cascade step.⁴⁰ The distributions from the interaction of 378-MeV protons with U^{238} , selected for several ranges of E^* , are shown in Fig. 8. The angular distribution of angular momentum vectors is symmetric about 90° within statistical errors, which justifies the use of $|\cos\theta|$ in the figure. Results using the nuclear model STEP³⁵ were qualitatively the same as those using STEPNO.³⁵ Figure 8 shows a preferential orientation of the angular momentum vectors for events with $E^* < 50$ MeV at values of $|\cos\theta|$ near unity or at angles near 0° and 180° . Approximately 110 mb of cross section is contained in the shaded area of the peak. These events are not associated with abnormally low values of angu-

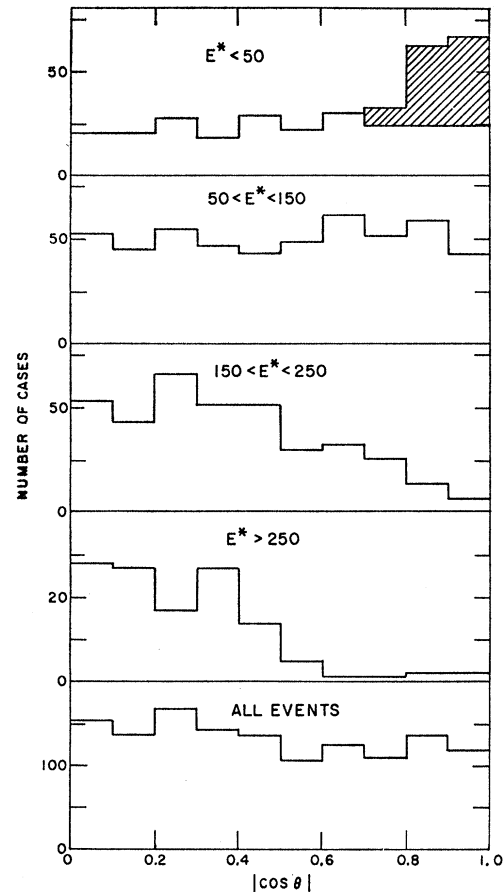


FIG. 8. Angular distribution of angular momentum vectors for selected bins of deposition energies. Results are based on the calculations of Chen *et al.* (see Ref. 34) for the interaction of 378-MeV protons with uranium using the nuclear model STEPNO.

lar momentum compared with other events of comparable E^* .

Halpern⁴¹ has proposed that a specific type of nucleonic cascade is responsible for the negative anisotropies in high-energy fission, namely, glancing collisions between the incident proton and a bound nucleon in which a single particle escapes from the nucleus with a small deflection and the other collision partner is captured. The over-all effect should be close to that which would have resulted from bombarding with a beam of low-energy particles moving perpendicularly to the beam direction. Examination of the Monte Carlo calculations³⁴ indicates that the shaded peak in Fig. 8 is predominantly due to cascades of the single-particle-out type when the nuclear model STEP is used. However, if the STEPNO model is used, cascades of the two-particle-out type contribute significantly to the peak as well.

Turning now to larger deposition energies, Fig. 8 indicates the distribution of angular momentum vectors is isotropic for $50 < E^* < 150$ MeV. As E^* is further

³⁶ A. Bohr, in *Proceedings of the First International Conference on the Peaceful Uses of Atomic Energy* (United Nations, New York, 1956), Vol. 2, p. 151.

³⁷ I. Halpern and V. M. Strutinski, in *Proceedings of the Second International Conference on the Peaceful Uses of Atomic Energy* (United Nations, Geneva, 1958), Vol. 15, p. 408.

³⁸ P. A. Goritchev, V. F. Darovskikh, O. V. Lozhkin, A. I. Obukhov, N. A. Perfilov, and U. P. Jakovlev, *Phys. Rev.* **126**, 2196 (1962).

³⁹ H. G. de Carvalho, G. Potenza, R. Rinzivillo, E. Sassi, and G. Vanderhaeghe, *Nuovo Cimento* **25**, 880 (1962).

⁴⁰ We are indebted to K. Chen for supplying a magnetic tape of the cascade outputs for these calculations.

⁴¹ I. Halpern, *Nucl. Phys.* **11**, 522 (1959).

TABLE V. Mean momenta in units of (MeV amu)^{1/2} for selected neutron-excess products of the interaction of uranium with protons of various energies.

Proton energy (GeV)	Isotope and N/Z value							
	Ba ¹⁴⁰ 1.500	I ¹³¹ 1.472	Pd ¹¹² 1.435	Mo ⁹⁹ 1.357	Sr ⁹¹ 1.394	Br ⁸³ 1.371	Zn ⁷² 1.400	Cu ⁶⁷ 1.310
0.4-0.7	134, ^a 132 ^b	131, ^c 134 ^d	131, ^b 127 ^d	129, ^b 126 ^d	130 ^b	102 ^c	119 ^b	111, ^b 106 ^d
2-6	133, ^e 133 ^a	131 ^d	120 ^d	125, ^a 120 ^d	125 ^e	96 ^d
18	...	120 ^e	95 ^e

^a Reference 12.^b Reference 11.^c Reference 18.^d Reference 13.^e This work.

increased a preferential orientation for low values of $|\cos\theta|$ develops. Naturally, in the limit of compound-nucleus formation all events would have $\cos\theta=0$. It is interesting to note that some preferred orientation of the angular momentum vectors perpendicular to the beam direction can be seen for events in which E^* is as low as $\approx \frac{1}{2}E_{\max}$. The distribution for all events, unselected on the basis of E^* , is not far from isotropic. The Monte Carlo calculation then predicts qualitatively the same dependence of b/a on E^* as is seen in the experimental data at 0.45 GeV. These comparisons could be made quantitative by detailed application of the theory of Halpern and Strutinski.³⁷

The calculations of Chen *et al.*³⁴ have not been extended to GeV energies, hence the graphs comparable to Fig. 8 are not available for 2.2-GeV protons. It is reasonable to expect the nature of cascades leading to low values of E^* will not change greatly with increased bombarding energy and perhaps the distribution of angular momentum vectors will not differ from that for $E^* < 50$ MeV in Fig. 8. The observed negative anisotropy of Ba¹⁴⁰ at 2.2 GeV tends to indicate this is the case.

The histograms of Fig. 8 show that a product such as Ba¹³¹ or Pd¹⁰³ having a deposition energy of several hundred MeV would be expected to show a pronounced positive anisotropy at a bombarding energy of 378 MeV. However, these values of E^* represent a much smaller fraction of E_{\max} in the case of irradiations by 2.2-GeV protons and we expect that they can be produced by a much greater variety of cascades. This could then account for a more nearly isotropic distribution of angular momenta and the nearly isotropic angular distributions of Ba¹³¹ and Pd¹⁰³ at 2.2 GeV.

C. Mean Momenta

In preceding sections we have seen that deposition energies and anisotropies depend on the N/Z of the observed product. However, the experimental data are not sufficient to divide middle mass products of uranium fission into two groups. The clearest evidence for such a distinction comes from the charge-dispersion measurements of mean ranges, particularly those of Brandt¹⁸ at 18 GeV. In this section we will discuss momenta to avoid the implicit dependence of range on the nature of the stopping medium. Use of momentum rather than

energy or velocity is appropriate for a fissionlike process, for, in the binary division of an excited nucleus, the momentum spectra of the two fragments in the moving system must be identical. Post-fission particle emission may weaken this equality somewhat.

In Table V we compare mean momenta obtained from the 90° spectra of the neutron-excess products of the present experiment with those from various thick-target measurements. Entries have been placed in three groups on the basis of bombarding energy: 0.38 to 0.72 GeV, 2.0 to 6.2 GeV, and 18 GeV. There is no strong evidence for an energy dependence within each group. Isotopes included in this table range from Ba¹⁴⁰ to Cu⁶⁷, and they are species which may be considered "conventional" low- or high-energy fission products. Agreement between results of different experiments is remarkably good. Entries for 0.4-0.7 GeV are nearly constant for isotopes from Ba¹⁴⁰ to Sr⁹¹ and then decrease for Zn⁷² and Cu⁶⁷. The value obtained by Brandt¹⁸ at 0.55 GeV for Br⁸³ appears anomalously low by comparison with this trend. As the bombarding energy increases into the GeV region, mean momenta of Ba¹⁴⁰ and I¹³¹ are virtually unchanged, but the lower mass products show small decreases in mean momenta. Brandt's results would indicate a lower mean momentum for I¹³¹ at 18 GeV than at 2-6 GeV. It is believed that at 2-6 GeV the mean momenta of products such as Pd¹¹², Mo⁹⁹, and Sr⁹¹ are significantly lower than those of Ba¹⁴⁰ and I¹³¹.

Mean momenta for some typical neutron-deficient isotopes from Ba¹³¹ to Br⁷⁶ are listed in Table VI together with data for some of the lower mass products from Cu⁶⁴ to Na²⁴. These lighter species, although neutron excess, have N/Z values in the same range as the heavier neutron-deficient products. Momenta of Ba¹³¹ and I¹²³ at 0.4-0.7 GeV are only slightly lower than those observed for Ba¹⁴⁰ and I¹³¹. However, increasing the bombarding energy results in a pronounced decrease in momenta for these products. Momenta of Mg²⁸ and Na²⁴ are low but show essentially no variation with energy.

In Fig. 9 we examine the dependence of mean momentum on the effective N/Z for products in the mass-140-to-119 range. Data from Friedlander *et al.*,¹² at 0.38 GeV, Sugarman *et al.*,¹¹ at 0.45 GeV, Brandt,¹⁸ at 0.55 GeV, and Alexander *et al.*,¹³ at 0.72 GeV agree well. Their trend is shown by the solid line in Fig. 9 and

TABLE VI. Mean momenta in units of $(\text{MeV amu})^{1/2}$ for neutron-deficient and low-mass products.

Proton energy (GeV)	Isotope and N/Z value								
	Ba ¹³¹ 1.339	I ¹²³ 1.321	Pd ¹⁰³ 1.239	Br ⁷⁶ 1.171	Cu ⁶⁴ 1.207	Mn ⁵⁶ 1.240	Sc ^{47,48} 1.262	Mg ²⁸ 1.333	Na ²⁴ 1.182
0.4-0.7	117 ^a	122, ^b 129 ^c	...	107 ^b	...	100 ^d	88 ^d	69 ^e	47 ^e
2-6	96, ^f 104 ^a	95, ^e 94 ^c	104 ^f	...	80 ^e	66 ^e	52 ^e
18	...	94, ^b 72 ^b	...	62 ^b

^a Reference 12.^b Reference 18.^c Reference 13.^d Reference 11.^e Reference 4.^f This work.

indicates momenta decreasing from $\approx 135 (\text{MeV amu})^{1/2}$ for the most neutron-excess species to $\approx 120 (\text{MeV amu})^{1/2}$ for the most deficient. The dashed line and points labeled 18 GeV are from the measurements of Brandt. It should be noted that the two entries for I¹²³ at 18 GeV in Table VI, 72 and 94 $(\text{MeV amu})^{1/2}$ represent values for I¹²³ formed cumulatively and independently, respectively. This indicates a rapid variation of mean momentum with N/Z at an N/Z value of 1.32 as shown by the dashed line. Other entries in Table VI for Ba¹³¹ and I¹²³ represent cumulative yields as a consequence of irradiation and separation times.

From Table VI and Fig. 9 it can be inferred that the mean momentum of a neutron-deficient product such as Ba¹³¹ decreases with increase of the bombarding energy from ~ 0.7 to 2.2 GeV, and that there is a further decrease between 2.2 and 18 GeV. It might be argued that Ba¹³¹ is not a good case for discussion as it is relatively close in N/Z to the region where momenta vary rapidly with N/Z . Indeed, the N/Z of Ba¹³¹ uncorrected for β -decay feeding is 1.339, which would place it to the right of the rise in the dashed curve in Fig. 9. To check this possibility, Bächmann and Cumming⁴² have measured the mean ranges of Ba¹²⁸, Ba¹³¹, and Ba¹⁴⁰ at 90° to beam in an experiment virtually identical to the present work. Only a small decrease in mean momentum between Ba¹³¹ and Ba¹²⁸ was observed, as is shown in Fig. 9, hence we conclude that the decrease in mean momentum between 2-6 GeV and 18 GeV is not due to some particular property of Ba¹³¹. The 2-6-GeV data by themselves are not sufficient to say whether the transition from the higher momenta of the neutron-excess products to the lower values for the deficient products is as abrupt as it is at 18 GeV.

D. Fission versus Spallation

In an idealized situation, distinction between fission and spallation as formation mechanisms for a particular product should be possible on the basis of momentum spectra. The kinetic energy of a fission fragment is produced by Coulomb repulsion, hence we expect high mean momenta and relatively narrow momentum distributions. On the other hand, in spallation a product's momentum is the sum of many small momentum kicks. Because of the essentially random orientation of the emitted particles, substantial cancellation of these

kicks is expected⁴³ and a spallation product's mean momentum should be lower and its spectrum broader than if it had been formed by fission.

In the de-excitation of highly excited nuclei such distinction will become less clear. Emission of relatively heavy particles in the evaporation cascade will tend to raise the momentum of a spallation product and lead to a relatively narrower spectrum. Substantial pre- and post-fission particle emission will have the opposite effect in fission. This can account for the small decrease of mean momentum with decreasing N/Z seen in Fig. 9 for products of fission induced by 0.4-0.7-GeV protons.

The neutron-excess products observed in this work (Ba¹⁴⁰, Mo⁹⁹, and Sr⁹¹) are characterized by narrow momentum distributions and mean momenta which are little changed from those observed at energies of 0.45 GeV. There is little doubt that these products arise from fission processes very similar to those postulated by Sugarman *et al.*,¹¹ to account for yields in the mass-47-to-140 range at 0.45 GeV. The observation that a negative anisotropy persists in the angular distribution of Ba¹⁴⁰ up to 2.2 GeV suggests that this and similar highly neutron-excessive products are formed as the result of rather simple fast nucleonic cascades, which are associated with low deposition energies and probably an asymmetric mass division in the fission process.

It is expected that the partner fragments to Ba¹⁴⁰ should be found in the mass-90-to-100 region. However, negative anisotropies are not observed in that region at

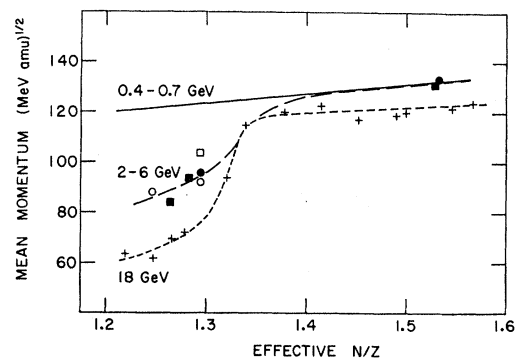


FIG. 9. Dependence of mean momentum on effective N/Z of the product. Data points are from: ●, the present experiment; ○, Bächmann and Cumming (Ref. 42); ■, Alexander *et al.* (Ref. 13); □, Friedlander *et al.* (Ref. 12); and +, Brandt (Ref. 18).

⁴² K. Bächmann and J. B. Cumming (unpublished).

⁴³ C. Hsiung, H. Hsiung, and A. A. Gordus, *J. Chem. Phys.* 34, 535 (1961).

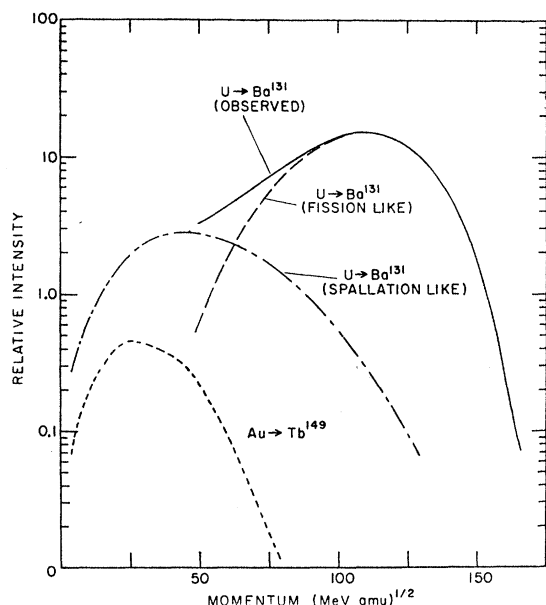


FIG. 10. Momentum spectra at 90° to the beam for Ba^{131} from uranium and Tb^{149} from gold irradiated with 2.2-GeV protons. The spectrum for Ba^{131} production from uranium by a spallationlike mechanism has been inferred from the Tb^{149} spectrum. This has been subtracted from the observed Ba^{131} spectrum to give a fissionlike spectrum.

0.45 GeV¹¹ and our data at 2.2 GeV for Mo^{99} and Sr^{91} show slightly lower mean momenta and broader distributions than those of Ba^{140} . It is reasonable to expect that Mo^{99} ($N/Z=1.357$) will accumulate fission products having a much wider range of N/Z values than would Ba^{140} ($N/Z=1.500$). The higher average deposition energy of Mo^{99} (see Fig. 7) is expected to be associated with fissioning species of lower charge and with increased post-fission evaporation, both effects leading to lower momenta. While some contribution from a Ba^{140} -like spectrum is consistent with the high-momentum side of the Mo^{99} spectrum, the dominant contribution to Mo^{99} appears to be due to more symmetric, higher-deposition-energy fission processes. We have noted that Mo^{99} will accumulate $\approx 70\%$ of the total isobaric yield at mass 99. Furthermore, the yield at this mass is not much below that at the peak of the fission-yield curve.⁸ We expect then that Mo^{99} should be quite typical of the low and medium energy fission processes induced in uranium by 2.2-GeV protons. On the other hand, Ba^{140} is representative of low-deposition-energy fission.

Turning now to the more interesting neutron-deficient products (Ba^{131} and Pd^{103}), we have seen that these are characterized by higher deposition energies, a substantial decrease of mean momenta with increased bombarding energy, and generally broader momentum spectra than the neutron-excess species. Of particular interest is the relative large number of low-momentum recoils [< 50 (MeV amu)^{1/2}] in the case of Ba^{131} . Rudstam and Sorensen¹⁴ have suggested that the highly

neutron-deficient iodine isotopes are produced from uranium at 18 GeV by a spallationlike mechanism. Their conclusion is based on the observation that the difference between the yield versus mass number curves representing iodine isotopes produced from uranium at 18 and at 0.59 GeV is very similar to the observed yield curve for iodine isotopes from gold or lower mass targets at 18 GeV. Comparison of momentum spectra of Ba^{131} or of Pd^{103} observed in the present work with those expected for spallation reactions (as inferred from data on Tb^{149} production from various targets)^{27,44} allows semiquantitative estimation of the magnitude of spallation contributions at these mass numbers.

The momentum of a spallation product is the vector sum of the momenta of the various emitted particles. For products far removed from the target, it is expected⁴³ that the mean magnitude of the recoil momentum will depend to a rough approximation on the square root of the number of nucleons, ΔN , separating the target and product, provided the energy spectra and relative numbers of nucleons, α particles, etc. does not change. A test of this approximation may be made using the results of recoil studies of Tb^{149} by Winsberg.²⁷ From his data at 3 GeV, values of $\langle P \rangle / (\Delta N)^{1/2}$ are calculated to be 4.82, 4.92, and 4.93 (MeV amu)^{1/2} for Ta, Au, and Bi targets, respectively. Reasonable extrapolation from these values predicts mean momenta of 53 and 59 (MeV amu)^{1/2} for Ba^{131} and Pd^{103} formed by a spallationlike mechanism from U^{238} . While many factors have been ignored in this treatment, these values are substantially lower than the observed momenta and it does not seem that spallation, as represented by Tb^{149} production from gold, can account for all Ba^{131} or Pd^{103} production at 2.2 GeV. However, the observed momenta of neutron deficient iodine isotopes at 18 GeV are not far from those predicted for spallation residues; this tends to support Rudstam and Sorensen's conclusion at the higher energy.

Quantitative estimation of the contribution of spallation to Ba^{131} production is possible by the use of a similar extrapolation of the momentum spectra of Tb^{149} . The short-dashed curve in Fig. 10 is the momentum spectrum of Tb^{149} recoils from a thin gold target observed at 90° to a beam of 2.2-GeV protons.⁴⁴ The mean momentum, 32 (MeV amu)^{1/2}, is in reasonable agreement with the value obtained by Winsberg.²⁷ The solid curve in Fig. 10 is the momentum spectrum of Ba^{131} observed at 90° to the beam in the present work. The dot-dashed curve has been obtained from the Tb^{149} spectrum by multiplying each abscissa value by 1.65, so that its mean is increased to 53 (MeV amu)^{1/2}. The height of the dot-dashed curve has been adjusted so that it accounts for all the Ba^{131} observed with momenta less than 50 (MeV amu)^{1/2}. The area of the dot-dashed curve is 18% that of the total Ba^{131} . Subtraction of this

⁴⁴ V. P. Crespo, J. B. Cumming, and J. M. Alexander (unpublished).

“spallationlike” contribution leaves the narrower “fissionlike” spectrum whose mean momentum is ≈ 107 (MeV amu) $^{1/2}$. Similar resolution procedures indicate that a somewhat larger contribution is made by spallation to the Ba^{131} spectrum observed at 15° and a smaller one to the spectrum at 165° . This implies an F/B ratio for the spallation contribution which is greater than the average $F/B=1.33$ observed for Ba^{131} , in agreement both with the generally larger F/B ratios observed for Tb^{149} production and with the larger F/B ratios of low-velocity Ba^{131} recoils inferred from our analysis of correlations between $v_{||}$ and V in Sec. II D.

At $A=131$, Ba^{131} represents about one-third of the total isobaric yield. Another third, the neutron-excess products similar to Ba^{140} , shows no contribution from spallation. Based on the cumulative cross section for forming Ba^{131} at 2.9 GeV, 8.6 mb 12 of which $\approx 18\%$ is spallation, with the assumption that the spallation contribution from the missing third of the yield is equal to that for Ba^{131} , we infer that spallation contributes less than ≈ 3 mb to the total yield, 28 mb, 12 at mass 131. Spallation is also only a rather small part of the ≈ 16 mb estimated by Friedlander *et al.* 12 to lie under the neutron-deficient peak of the charge-dispersion curve.

We have noted that the Pd^{103} spectra contain relatively fewer low-momentum recoils than do the Ba^{131} spectra. For momenta less than 50 (MeV amu) $^{1/2}$ the values are 2.4% for Pd^{103} compared to 8.6% for Ba^{131} in the case of the 90° spectra. Analysis of the Pd^{103} spectra in a manner similar to that described for Ba^{131} indicates an $\approx 6\%$ contribution of a spallationlike process. After subtraction, the remaining fissionlike part has a mean momentum of ≈ 107 (MeV amu) $^{1/2}$. Pd^{103} , with a cross section of 3.6 mb at 2.9 GeV, 16 represents only $\approx 10\%$ of the isobaric yield at $A=103$. On the other hand, some 70% of the yield (represented by products such as Mo^{99}) has very little if any spallation contribution. We estimate then that the spallation contribution at $A=103$ should not be greater than three times that of Pd^{103} alone, or ≈ 0.6 mb. While the above discussions are rather qualitative, two conclusions seem secure: Spallation at 2.2 GeV is not a major contributor to yields at either $A=131$ or $A=103$, and the contribution at $A=131$ is greater than at $A=103$. The second of these, when combined with the observed rapid decrease of the mass-yield curve with increasing mass number in the vicinity of $A=131$, 8 leads to the prediction that spallation should become a relatively more important and possibly dominant mechanism in the rare-earth region. The continued decrease of mean momenta of a product such as Ba^{131} from 2.2 to 18 GeV indicates that spallation will make a greater contribution to middle mass products at the higher energy.

E. Energetics of Fission

Having noted that the observed spectra of products such as Ba^{131} and Pd^{103} can be interpreted in terms of a

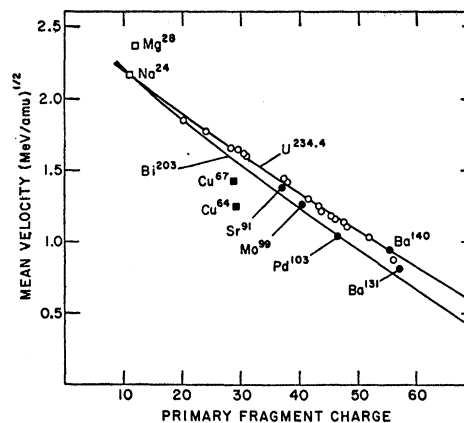


FIG. 11. Dependence of mean velocity on the charge of the primary fission fragment. The curves have been calculated using the theory of Nix and Swiatecki (Ref. 45), for $U^{234.4}$ and Bi^{203} as fissioning species. The experimental points are from: ●, the present experiment; ○, Sugarman *et al.* (Ref. 11); ■, Alexander *et al.* (Ref. 13); and □, Crespo *et al.* (Ref. 4).

fission mechanism with some spallation contribution, the next question to examine is to what extent the fission process at 2.2 GeV is different from that at lower energies. It has been shown it is not necessary to invoke a fast time scale process to account for the spectra and angular distributions of Ba^{131} and Pd^{103} , despite the rather large deposition energies involved in their formation at 2.2 GeV. We will use the simplified liquid-drop treatment developed by Nix and Swiatecki 45 as a framework for the discussion which follows. In their theory the nucleus prior to scission is treated as two overlapping spheroids. We have used $U^{234.4}$ to represent a typical fissioning nucleus at low bombarding energies. This is the same fissioning species postulated by Sugarman *et al.* 11 for their observations at 0.45 GeV and is a reasonable choice based on Monte Carlo calculations and subsequent pre-fission evaporation.

Examination of the mass, charge, and deposition energy (A, Z, E^*) distributions from Monte Carlo calculations 33 indicates that the most pronounced change which occurs as the bombarding energy is increased from 0.45 to 1.83 GeV is in the frequency of cascades leading to products of charge and mass far removed from those of the target. For example, only 0.4% of the cascades at 0.45 GeV lead to products with $Z < 90$. The figures rises to 7% at 0.96 GeV and to 30% at 1.83 GeV. The average product nucleus of these large cascades at 1.83 GeV is Ra^{228} with a deposition energy of 500 MeV. The evaporation calculations of Dostrovsky *et al.* 46,47 suggest that such a nucleus prior to fission will lose on the average some 25 nucleons of which ≈ 5 will be charged. We will therefore use Bi^{203}

45 J. R. Nix and W. J. Swiatecki, Nucl. Phys. 71, 1 (1965).

46 I. Dostrovsky, P. Rabinowitz, and R. Bivins, Phys. Rev. 111, 1659 (1958).

47 I. Dostrovsky, Z. Fraenkel, and P. Rabinowitz, in *Proceedings of the Second International Conference on the Peaceful Uses of Atomic Energy* (United Nations, Geneva, 1958), Vol. 15, p. 301.

as a representative nucleus for high-deposition-energy fission. Both the prompt and evaporation cascade calculations predict very broad distributions in A and Z so that Bi^{203} will be at best a reasonable guess for an average fissioning species.

In Fig. 11 we present curves giving the dependence of mean velocity V_1 of a primary fission product on the primary fragment charge Z_1 as calculated for the fissioning species $\text{U}^{234.4}$ and Bi^{203} using the theory of Nix and Swiatecki.⁴⁵ As a first approximation for not too asymmetric fissions the variation can be represented by straight lines of the form

$$\langle V_1 \rangle = (1 - Z_1/Z_f)(8E^\circ/A_f)^{1/2},$$

where Z_f and A_f are the charge and mass of the fissioning nucleus. E° is a constant for a particular A_f and Z_f , predicted by the theory to be 164 MeV for $\text{U}^{234.4}$ and 146 MeV for Bi^{203} . More exact treatment leads to the curves shown in Fig. 11 which are concave upwards for the products of lower charge (more asymmetric fissions). In the Nix and Swiatecki model calculations it is assumed that $A_1/Z_1 = A_f/Z_f$.

Post-fission particle evaporation does not change fragment velocities to an appreciable extent, hence we can compare observed velocities directly with those predicted for the primary fragments. We have included corrections for feeding by β decay based on charge-dispersion curves but have assumed only neutrons are emitted after fission in estimating the charge of the primary fragment corresponding to a particular observed product. The open circles in Fig. 11 are the results obtained by Sugarman *et al.*¹¹ at 0.45 GeV. Agreement with the line calculated for $\text{U}^{234.4}$ as the fissioning species is very good, the root-mean-square deviation of a point being $< 2\%$. This serves to confirm in a somewhat different way the conclusion drawn by Sugarman *et al.* that fission of uranium at 0.45 GeV does not involve any process fundamentally different from that in fission produced by heavy ions, α particles, etc., at lower energies.

Turning now to the results of the present experiment at 2.2 GeV, mean velocities for Sr^{91} , Mo^{99} , Pd^{103} , Ba^{131} , and Ba^{140} (from the 90° spectra) are plotted as filled circles in Fig. 11. Values for Pd^{103} and Ba^{131} have been corrected for the contribution of spallation. The point for the most neutron-excessive product observed in this work, Ba^{140} , falls directly on top of the point for the same nuclide at 0.45 GeV, which tends to indicate a similar fissioning nucleus at both energies. We had concluded previously on the basis of the observed negative anisotropy of the angular distribution that Ba^{140} was formed from the products of rather simple, low-deposition-energy cascades; Fig. 11 gives added evidence for this point.

Velocities of the four other products fall below the line calculated for $\text{U}^{234.4}$ as the fissioning species, which may be taken as indicating contributions from fissioning

species having charges less than 92. The most neutron-deficient product, Pd^{103} , falls very close to the line calculated for our representative high-deposition-energy fission species, Bi^{203} . We conclude then that fission induced by 2.2-GeV protons which leads to products in the $Z = 35$ to 60 region is fission, not significantly different from that at lower energies, provided that the range of charges of fissioning species is considered and that correction is made for a spallation contribution to the more neutron-deficient products.

The filled squares in Fig. 11 are the results for Cu^{64} and Cu^{67} obtained by Alexander *et al.*¹³ at 6.2 GeV. While the mean velocities of Cu^{67} , Zn^{72} , Ga^{72} , and Ga^{73} observed at 0.45 GeV¹¹ agree with those predicted by the theory, the values for Cu^{64} and Cu^{67} at 6.2 GeV fall well below even the curve calculated for Bi^{203} as a fissioning species. We concur with the conclusion of Alexander *et al.* that their formation at 6.2 GeV involves a significant contribution of a nonfissionlike process. An alternative explanation, that of extensive post-fission charged-particle emission, seems unreasonable particularly in the case of Cu^{64} .

The general shape of the curves drawn in Fig. 11 indicates that for different values of Z_f the curves tend to intersect for fragment charges below 20. Hence, the relative dependence of fragment velocity on charge of the fissioning species will be greater for products of higher charge than for lower charged ones. It is interesting to note that extrapolation of the calculated curves to low charges predicts approximately correct mean velocities for light fragments. We have plotted the experimental points for Na^{24} and Mg^{28} taken from the 3-GeV results of Crespo *et al.*⁴ at $Z = 11$ and 12, respectively. Charged-particle emission probably cannot be ignored for these low masses, hence both points should be shifted somewhat to the right in the figure. We do not wish to imply that a fissionlike mechanism is responsible for Na^{24} and Mg^{28} production but only to note that their velocities are not very different from those predicted by a separation distance, between charges at the time of scission, close to that in ordinary fission. Although the Nix and Swiatecki⁴⁵ calculations apply only to the more symmetric mass divisions, Swiatecki⁴⁸ points out that the potential energy surface decreases again for very asymmetric mass division and can give rise to high yields of both the spallation residues and these emitted light products. Detailed calculations, however, have not been carried out.

An interesting consequence of this theoretical treatment of fission is the insensitivity of the mean fission fragment velocity to either charge or mass of the fissioning species. As shown in Fig. 11, the mean velocity is $1.18(\text{MeV amu})^{1/2}$ for $\text{U}^{234.4}$ as the fissioning nucleus and 1.19 for Bi^{203} . Since our data for fission involving a wide range of deposition energies are consistent with the

⁴⁸ W. J. Swiatecki (private communication); S. Cohen and W. J. Swiatecki, *Ann. Phys. (N. Y.)* **19**, 67 (1962).

theory, we are led to predict that direct experimental measurement (for example by time of flight) of the mean velocity of fragments from the GeV proton-induced fission of uranium should give a result close to 1.2. On the other hand, if the experiment were to include contributions from nonfission processes, e.g., Cu^{64} , we would expect a lower value.

IV. CONCLUSIONS

The dominant process leading to the formation of products having masses between ≈ 90 and ≈ 140 from uranium targets irradiated by 2.2-GeV protons is binary fission. The observation of low-momentum recoils in the spectra suggests some contribution from a spallationlike process to products having N/Z less than ≈ 1.35 . The observed spectra and angular distributions of even the neutron-deficient products Pd^{103} and Ba^{131} are shown to be consistent with the assumption of a two-step mechanism for their formation. There are no detectable inconsistencies of the sort observed in a previous study of a typical fragmentation reaction, Na^{24} production from bismuth by 2.9-GeV protons, hence it is not necessary to postulate reactions on a fast time scale to account for Pd^{103} and Ba^{131} production.

Fission of uranium by 2.2-GeV protons involves wide ranges of deposition energies and fissioning species. Based on narrow momentum spectra, negative anisotropies of the angular distribution, and low values of E^* it can be concluded that a highly neutron-excess product such as Ba^{140} is produced, on the average, by the fission of nuclei rather close in A and Z to the target which arise from simple fast nucleonic cascades and limited pre-fission evaporation. Less neutron-excess or somewhat neutron-deficient products— Sr^{91} , Mo^{99} , and Ba^{131} —are

formed from fissioning species further removed from the target. There is a strong inverse correlation of the cascade deposition energy E^* with the N/Z of the fission product. Properties of the most neutron-deficient product studied in this work, Pd^{103} , are consistent with a deposition energy of 400 MeV and a fissioning species of charge ≈ 83 . Provided the wide range of charges of fissioning species resulting from the prompt cascade and pre-fission evaporation are considered, mean velocities of the observed products can be accounted for by a liquid-drop theory of the type used to interpret fission induced by α particles and heavy ions. There is no need to postulate abnormal saddle or scission point configurations; and fission, even at those excitation energies reached in 2.2-GeV proton irradiations, is the same as at substantially lower energies.

ACKNOWLEDGMENTS

The authors are indebted to their colleagues for many helpful discussions and suggestions during the present work. One of us (V.P.C.) wishes to acknowledge the hospitality of the Brookhaven National Laboratory Chemistry Department during the time he spent there. He would like to thank the Luso-American Educational Commission of Lisbon for a Fulbright grant, and the University of Coimbra and the Portuguese I. A. C. for permission for the leaves. The performance of the numerous chemical yield analyses by the group headed by Dr. R. W. Stoenner, and the preparation of the targets by the group headed by R. Withnell, are gratefully acknowledged. We wish to thank Dr. H. Rylander for his assistance during some of the experiments. The continued cooperation of the cosmotron operating staff was most appreciated.